Transport mechanisms in silicon heterojunction solar cells with molybdenum oxide as a hole transport layer

R. García-Hernansanz[1]*, E. García-Hemme[1], D. Montero[1], J. Olea[1], A. del Prado[1], I. Mártil[1], C. Voz[2], L.G. Gerling[2], J. Puigdollers[2], R. Alcubilla[2]

[1]*Dept. de Física Aplicada III (Electricidad y Electrónica), Univ. Complutense de Madrid, 28040 Madrid, Spain*

[2] *Departament d'Enginyeria Electrònica. Universitat Politècnica de Catalunya. 08034 Barcelona (Spain)*

**corresponding author: rodgar01@ucm.es. Univ. Complutense de Madrid, 28040 Madrid, Spain*

Abstract:

Heterojunction solar cells based on molybdenum sub-oxide (M_oO_x) deposited on n-type crystalline silicon have been fabricated. The hole selective character of M_oO_x is explained by its high workfunction, which causes a strong band bending in the Si substrate. This bending pushes the surface into inversion. In addition, the sub-stoichiometry of the evaporated M_oO_x layers leads to a high density of states within the bandgap. This is crucial for charge transport. The J-V electrical characteristics at several temperatures were analysed to elucidate the dominant charge transport mechanisms of this heterojunction structure. We have identified two different transport mechanisms. At low bias voltage, transport is dominated by hole tunneling through the M_oO_x gap states. At higher voltage the behavior is similar to a Schottky junction with a high barrier value, due to the high M_oO_x work function. These results provide a better understanding of the hole selective

character of M_oO_x/n-type silicon heterocontacts, which is key to further improve this new kind of solar cells.

KEYWORDS: Molybdenum oxide, Multitunneling, gap states, heterocontact.

1. Introduction

The present record energy conversion efficiency of silicon-based solar cells is 26.3 % [1], which is close to the Shockley–Queisser limit for a single junction silicon solar cell [2]. Such a high efficiency has been achieved by Kaneka combining the HIT (Heterojunction with Intrinsic thin Layer) concept with an interdigitated back contact (IBC) structure. This record efficiency exceeds by 1% the best silicon homojunction solar cells [3]. Nevertheless, conventional silicon p-n junctions still dominate the solar cell market owing to their simpler fabrication, which enable lower manufacturing costs. The need of comparatively complex PECVD deposition systems and the need of hazardous precursors slow down the adoption of heterojunction technology.

A limitation of conventional two-side HIT solar cells is the parasitic light absorption of amorphous silicon layers, which reduces the photocurrent [4]. On the other hand, the absence of high temperature processes makes this technology more processing-friendly with thinner wafers, as opposed to conventional homojunction solar cells. These standard cells also have other limitations such as recombination losses [5] and heavy doping effects[6], which impose a limit on their efficiency.

In the last few years several works have been published aiming to replace doped emitters of classical Si junctions with alternative materials. The aim is to achieve a "carrier-selective" interface with the absorber [7],[8],[9]. The charge separation occurs because one type of charge is blocked while the flow of the opposite one is allowed[10]. The incorporation of such carrier selective heterocontact structures could improve some

fundamental limitations of conventional solar cells. Furthermore, most of these materials can be deposited by evaporation or even solution-processed[11]. If these simple technologies could be integrated in a commercial route then higher-efficiency cells could be cost-effectively manufactured. There are different materials reported in the literature that have demonstrated excellent carrier-selective properties on c-Si: organic films[12],[13], fluoride salts[8],[14] or transition metal oxides (TMOs)[15],[16]. At present, organic semiconductors are unstable when exposed to the atmosphere and suffer photodegradation effects[17]. For this reason, inorganic alternatives in combination with silicon absorbers are actively researched. Lithium fluoride[8],[18], and titanium dioxide[19] layers have been used as electron collectors on n-type Si substrates, while molybdenum oxide (MoO_x) and tungsten oxide (WO_x) have been used as hole collectors also for n-type Si[20],[21],[22]. Recently, a conversion efficiency of 22.5 % has been obtained for a solar cell with a MoO_x hole collector on n-type silicon[23]. However, this device still required a very thin intrinsic amorphous silicon layer between the silicon substrate and the MoO_x layer for interface passivation.

TMOs have been studied in depth for organic semiconductor devices[24],[25],[26], for electronic applications [27],[28] and more recently some works have studied these materials deposited on silicon heterojunctions. The physical principles explaining the collection of photogenerated charge-carriers in these devices have been proposed by Battaglia *et al.[22]*. Nevertheless, a deeper understanding of the mechanisms governing charge-carrier transport without illumination is still needed. An accurate analysis and understanding of the J-V electrical characteristics in dark can provide guidelines to improve the V_{oc} values of these devices.

2. Experimental methods

In Fig. 1 we present the structure of the MoO_x heterojunction solar cells studied in this work. The substrate was a double-side polished, 300 µm thick, n-type (2.5 Ω·cm) crystalline silicon wafer. First, the substrate was cleaned by a standard RCA cleaning process with a subsequent dip in HF solution (1%) until it became hydrophobic. Then, it was loaded into a PECVD system to deposit a stack of layers on the rear side. This stack consisted of a 4 nm intrinsic a-SiC_x:H (x~0.2) passivation layer and a 15 nm phosphorous-doped a-Si:H layer (15 nm). An additional stoichiometric a-SiC_x:H (x~1) layer was deposited to protect the stack and as a back reflector coating (BRC). Afterwards, the rear side was laser-fired to obtain an array of locally-diffused point contacts with a contacted area ratio of 0.5%. This optimized laser process allows to combine low series resistance with reduced surface recombination at the rear contact [29]. On the front side, after another HF dip, a 15 nm MoOx layer was thermally evaporated directly on the c-Si substrate, without an a-Si:H passivation layer. We cannot discard the presence a thin interfacial SiO_2 layer (~2 nm) between the Si substrate and the MoO_x that grows spontaneously[30]. Subsequently an indium-tin-oxide (ITO) front electrode was deposited by RF magnetron sputtering. Solar cells with 1 cm^2 and 4 cm^2 active area were defined by a lithographic process and a wet etching of the ITO and MoOx layers. The front electrode is finished by thermally evaporating a 2 µm thick silver grid. This electrode covers less than 5% of the device area. Finally, the rear electrode consisted in a 1 µm thick aluminium layer evaporated on the laser-fired contacts.

The current density as a function of applied voltage (J-V characteristic) was measured with an Agilent 2400 SourceMeter. The J-V curves were measured in darkness and under 1-sun AM1.5 illumination with an ORIEL 94021A (Newport) solar simulator. The light irradiance was properly calibrated by means of a pyrometer. The external quantum efficiency curve was measured using a commercial instrument QEX10 from PV

Measurements. After the initial room temperature characterization, the solar cell was mounted inside the chamber of a closed-loop helium cryostat, which controls temperature with an additional heater. Then, J-V characteristics in darkness were measured at temperatures from 360 K to 220 K. All these electrical measurements were done in a 4 wire configuration to minimize the contribution of the copper cables to the series resistance. The well-known two-diode model was used to fit the measured J-V curves[31],[32] according to the following expression:

$$J = J_{D1} + J_{D2} + J_{SHUNT}$$

$$J = J_{0,1}(T)\left[e^{A_1(T)(V-JR_S)} - 1\right] + J_{0,2}(T)\left[e^{A_2(T)(V-JR_S)} - 1\right] + \frac{V-JR_S}{R_{Shunt}} \qquad (1)$$

In this expression J_{D1} and J_{D2} correspond to the two main conduction mechanisms, where $J_{0,1}\ (T)$ and $J_{0,2}\ (T)$ are the saturation current densities and $A_1\ (T)$, $A_2\ (T)$ are the exponential factors of each mechanism. Also, the parasitic series resistance R_S and parallel resistance R_{Shunt} were considered in the equivalent circuit. We can determine the different conduction mechanisms by studying the temperature dependences of the fitting parameters of equation (1). It is known that the saturation current density and the exponential factor will adjust to the following expressions[33],[34]:

$$J_{0,i} = J_{0,0,i} \cdot e^{\frac{-E_{a,i}}{kT}} \qquad (2) \qquad\qquad A_i(T) = \frac{q}{n_i kT} \qquad (3)$$

where $E_{a,i}$ is the activation energy of each mechanism and n_i the corresponding diode ideality factor. Finally, to analyse the electrical characteristics measured at reverse bias polarization we used the following equation[31],[35]:

$$J_R = J_{rev,0} e^{\left(-\frac{E_{a,rev}}{KT}\right)} (V_D - V)^b \qquad (4)$$

where $J_{rev,0}$ is a base current, V_D a constant voltage, $E_{a,rev}$ an activation energy of the process and *b* is a temperature independent coefficient.

3. Results and discussion

Figure 2 shows the EQE and J-V characteristic curve of a representative MoO_x based solar cell at room temperature under 1-sun illumination. All the fabricated devices showed a similar behaviour, either for 1 cm^2 or 4 cm^2 cells. These solar cells have a V_{OC} = 614 mV, J_{SC} = 32,8 mA/cm^2 and F.F. = 73.2 %, resulting in a photovoltaic conversion efficiency of 14.7%. To our knowledge this is the best efficiency reported for a direct heterojunction between MoO_x and n-type c-Si without passivation layers. The V_{OC} and F.F. values are significantly higher than those previously reported[9]. Although the Jsc value is lower in our cells, but is rather good for a non-textured surface.

In Fig. 3 we present the forward J-V characteristics in darkness of a representative 1 cm^2 MoO_x based solar cell measured from 360 K to 220 K, at intervals of 20 K. In the same figure the blue lines represent the curves fitted to equation (1) for each temperature. We can observe the good agreement between the measurements and the fitted curves in all the temperature range. At high bias the effect of series resistance is observed, with values lower than 2 $\Omega \cdot cm^2$ for all curves. The shunt resistance is not observed in any of the curves measured under dark conditions. The curves present clearly two different slopes, at low bias (V < 0.4 – 0.6 V depending on the temperature) and at high bias (V > 0.4 – 0.6 V). This indicates that two different conduction mechanisms with exponential behaviour are taking place. In Fig. 4 we plot the parameters $A_1(T)$ (high voltage range) and $A_2(T)$ (low voltage range) obtained from the fittings. While $A_1(T)$ has a strong temperature dependence, $A_2(T)$ remains roughly constant. Fitting the high voltage mechanism to equation (3) we obtain a constant diode factor of n_1 = 1.20 ± 0.09. On the

other hand, if the same equation is used to fit $A_2(T)$ the obtained diode factor value is between 3 and 4 depending on temperature. The diode ideality factor, which is deduced from dark electrical characteristics, indeed has influence on the solar cell efficiency. A high n-value not only degrades the FF, but it is also a signal of higher recombination. Therefore, it can be related to lower open-circuit voltages and, as a consequence, reduced efficiencies. In fact, as the diode ideality factor increases (from the ideal value of n = 1), the voltage at the maximum power point decreases, and therefore the efficiency of the device [36]. As the V_{OC} value of our cells is 614 mV, the efficiency of the cell will be determined by the dominant transport mechanism at these voltage range, that is the one with n_1 = 1.20. Therefore, if we would like to obtain better efficiencies, we should obtain cells with lower diode factor in this process, close to n = 1. Concerning the other mechanism observed in the J-V characteristics, a temperature depended diode factor is common in trap-assisted tunneling processes [37]. This temperature dependence can be relate with an interface state density distribution [38, 39], quantum mechanical tunnelling [39, 40] or image force lowering [40]. In Fig. 5 we present the Arrhenius plots of the saturation current densities related to the high and low voltage processes. An activation energy (E_a) of 0.90 eV was obtained for the high voltage mechanism and an E_a = 0.30 eV was obtained for the low voltage one. These values clearly differ from a typical recombination diode and must be explained by other mechanisms. The high values of n_2, together with the moderate temperature dependence of A_2 and the E_a value of 0.3 eV, suggest that at low voltage the current is dominated by a tunnelling process [31]-[35].

In order to support this conclusion we analysed the electrical characteristics measured under reverse bias. In Fig. 6 we represent ln (J_R) vs ln (V) and these data are fitted to equation (4). A linear behaviour with very similar slope (b in equation (4)) is obtained for all measurements in the studied temperature range. The approximately

constant value obtained for the slope is b = 0.74 ± 0.03. By contrast, the intercept with the ordinate axis (when ln(V) = 0) shows a temperature dependence. In Fig. 7 we represent each intercept with the ordinate axis as a function of 1/T, and the linear fitting which results in an activation energy of $E_{(a,rev)}$=0.27 eV. This value for the activation energy, within experimental error, points to the same tunnel mechanism observed at low forward bias. These results are very relevant because the current measured in dark under reverse bias has the same direction as it has under illumination at low forward bias. Therefore, the conduction mechanisms taken place should be the same.

To explain these results, in Fig. 8 we present a qualitative band diagram of a MoO_x heterojunction solar cell, which can help to understand the conduction mechanisms of these devices. This figure is based on the band diagrams presented in Refs. [22],[41],[42]. The high work function of the MoO_x [16] produces a large band bending of the n-type silicon surface. In fact, an inversion layer appears at the interface with a hole concentration larger than the substrate doping concentration[21]. This p-type inversion layer near the surface is shown as the yellow region in Fig. 8. Furthermore, the MoO_x presents a high density of oxygen vacancies, which results in a quasi-continuous distribution of energy levels within its bandgap. In fact, Battaglia et al.[22] describe this quasi-continuous distribution of energy levels as a defect band. Other authors have referred to these gap states as a "quasi-conduction band" for oxides[28]. These states in the bandgap seem to play a capital role to explain the good hole injection and extraction properties of the MoO_x layer.

It has been suggested that the passivating behaviour of the MoOx layer is due to the spontaneous formation of an ultrathin SiO_x layer[30] between the Si substrate and the MoO_x. Since all the currents must flow across this SiO_x layer, the observed tunnelling mechanism in the J-V characteristic cannot be explained by processes within the SiO_x. If

that were the case, such tunnelling process would limit the current in the whole voltage range. Because of this, we conclude that the observed tunnelling process consists of holes transported across the MoOx gap states, labelled by (1) in Fig. 8. This tunnelling process is similar to that explained by Schulze et al.[31] for a-Si/c-Si heterojunction solar cells using the multitunnelling capture emission (MTCE) theory, where carriers from the c-Si tunnel into states within the amorphous silicon bandgap and then recombine through carrier capture or reemission. The saturation current density in MTCE is exponentially dependent on 1/T following an expression similar to Eq. 2.[43]. The activation energy of E_a=0.30±0.01 eV obtained from Fig. 5 by fitting the Arrhenius plot is consistent with the MTCE values reported in the study for different heterojunctions on silicon[31],[44]. The agreement between experimental results and the MTCE model supports our explanation of a tunnelling process dominant at low voltages.

On the other hand, there are two processes that could be related with a diode factor of n_1 = 1.20 and an activation energy of 0.90 eV: diffusion/recombination in the silicon bulk (labelled by (3) in Fig.8) and the transport of electrons between the c-Si and MoOx conduction bands (labelled by (2) in Fig.8). Although the obtained values are coherent with diffusion/recombination values reported for silicon heterojunctions[31], we believe that this cannot be the observed process. According to Fig. 3, the low voltage tunnelling process and this high voltage process operate in parallel, adding both currents. However, as it can be observed in figure 8, any transport process involving hole diffusion into the n-type c-Si would be in series with the hole tunnelling across the MoOx. The same applies for any process involving the recombination of electrons coming from the c-Si before they reach the MoOx. The only conduction process in parallel with the hole MoOx tunnelling is the injection of electrons from the c-Si over the barrier voltage into the MoOx conduction band.

As it can observed in Fig. 8, this structure is similar to a Schottky junction with a high barrier value due to the high MoOx work function. The strong inversion induced at the silicon surface explains the high activation energy of 0.9 eV. Concerning the diode ideality factor, a value of n = 1.20 is higher than that expected for Schottky barriers (n = 1). This higher value could be related with a voltage drop across the MoOx, and therefore it depends on its thickness[45].

4. Conclusions

We have fabricated a set of MoO_x solar cells with conversion efficiency of 14.7%, V_{OC} = 614 mV, J_{SC} = 32,8 mA/cm^2 and F.F. = 73.2 %. These values are lower than the state-of-the-art, but among the highest reported for direct MoO_x/n-type c-Si heterojunctions without any additional passivation layer. From the dark J-V characteristics as a function of temperature, two different transport processes were identified: a Schottky behaviour process with an ideality factor n_1 = 1.20, and a tunnelling process characterized by an ideality factor n_2 with values in the 3-4 range. This tunnelling process determines the electrical characteristic at low voltages. The exponential dependence of the saturation current density as a function of 1000/T suggests a multitunnelling capture emission process. We obtained an activation energy E_a=0.30$\pm$0.01 eV for this mechanism, which agrees with the MTCE model for silicon heterojunctions. Finally, when biased at high voltages and at usual operation temperatures, the current of these devices is mainly determined by the barrier between the MoOx and the c-Si conduction bands.

Acknowledgements:

Authors would like to acknowledge the CAI de Técnicas Físicas of the Universidad Complutense de Madrid for the use of its laboratories. This work was partially supported

by the Project MADRID-PV (Grant No. 2013/MAE-2780) funded by the Comunidad de Madrid, by the Spanish MINECO (Ministerio de Economía y Competitividad) under grants TEC 2013-41730-R, TEC2017-84378-R and ENE2016-78933-C4-1-R. Also by the Universidad Complutense de Madrid (Programa de Financiación de Grupos de Investigación UCM–Banco Santander) under grant 910173-2014. D. Montero acknowledges the Spanish MINECO (Ministerio de Economía y Competitividad) for financial support under contract BES-2014-067585 and L.G. Gerling the support from Mexico's grant program CONACyT.

Figure 1:

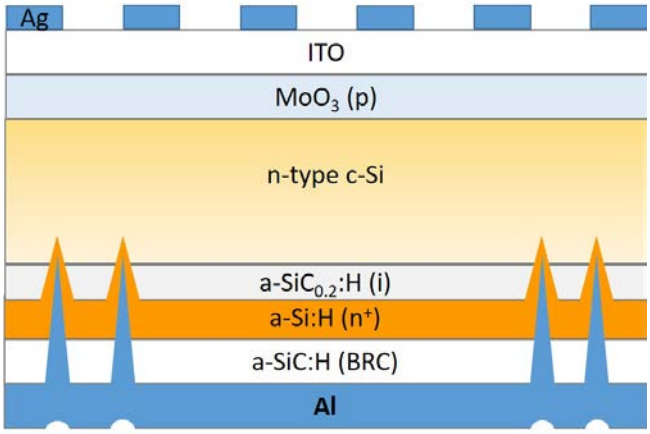

Figure 2:

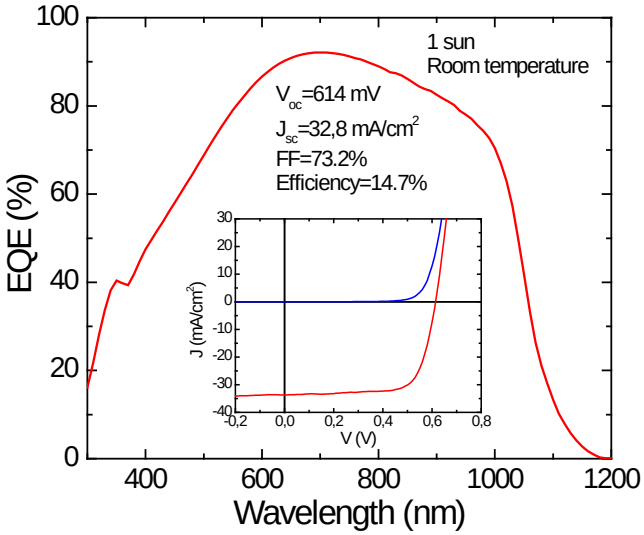
1 sun
Room temperature
V_oc=614 mV
J_sc=32,8 mA/cm²
FF=73.2%
Efficiency=14.7%
EQE (%)
Wavelength (nm)
J (mA/cm²)
V (V)

Figure 3:

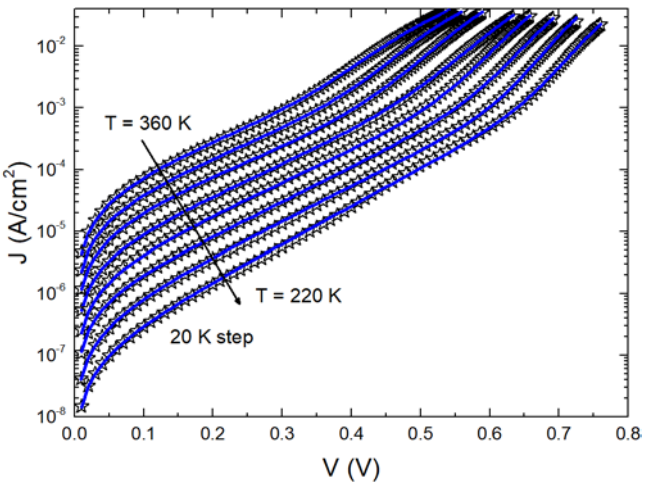
T = 360 K
T = 220 K
20 K step
J (A/cm^2)
V (V)
10^{-2}
10^{-3}
10^{-4}
10^{-5}
10^{-6}
10^{-7}
10^{-8}
0.0
0.1
0.2
0.3
0.4
0.5
0.6
0.7
0.8

Figure 4:

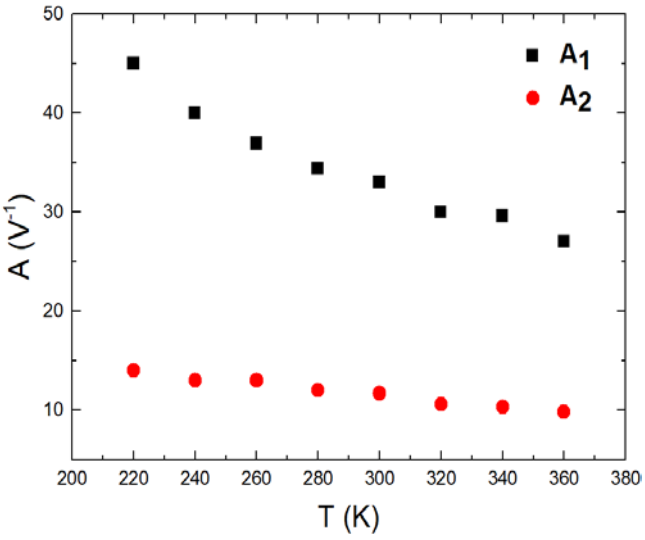

Figure 5:

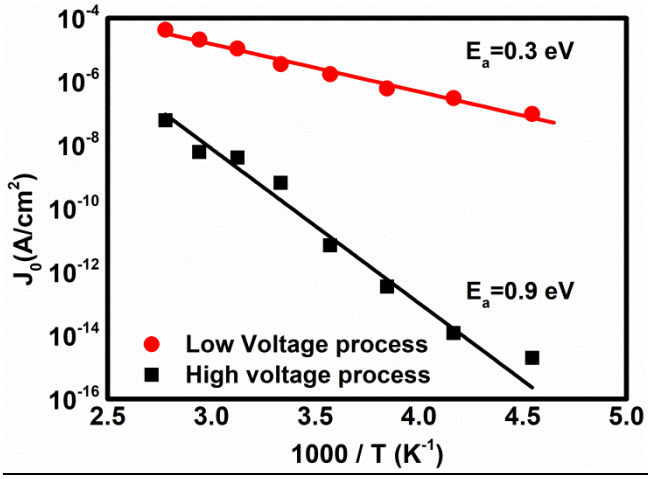
10^{-4}
10^{-6}
10^{-8}
10^{-10}
10^{-12}
10^{-14}
10^{-16}
J_0(A/cm^2)
2.5
3.0
3.5
4.0
4.5
5.0
1000 / T (K^{-1})
E_a=0.3 eV
E_a=0.9 eV
Low Voltage process
High voltage process

Figure 6:

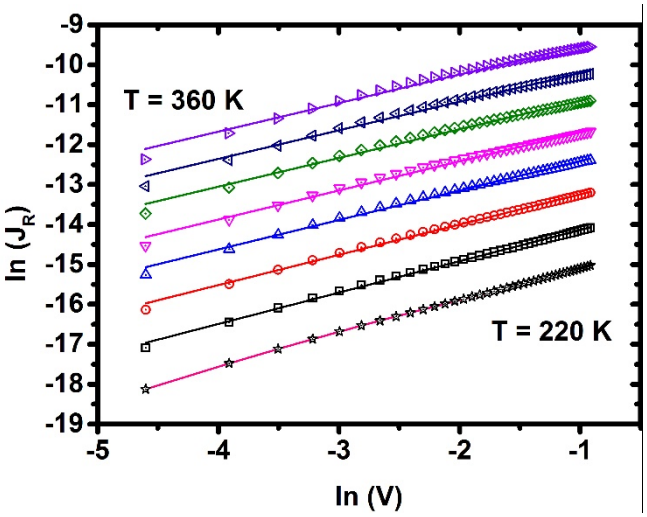

Figure 7:

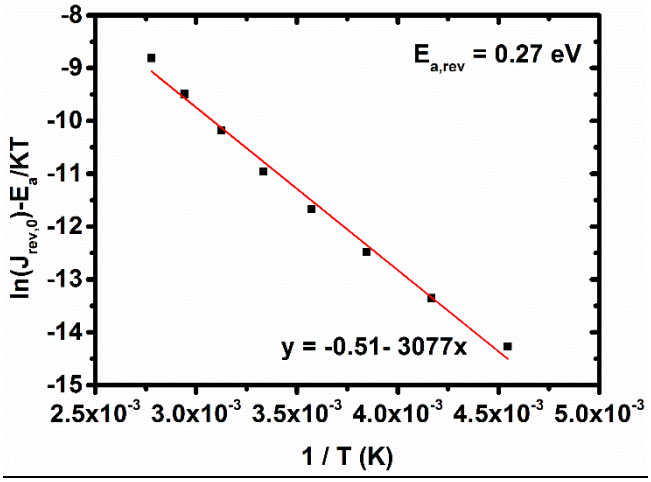
$E_{a,rev}$ = 0.27 eV
y = -0.51- 3077x
$\ln(J_{rev,0})-E_a/KT$
1 / T (K)
-8
-9
-10
-11
-12
-13
-14
-15
2.5x10^{-3}
3.0x10^{-3}
3.5x10^{-3}
4.0x10^{-3}
4.5x10^{-3}
5.0x10^{-3}

Figure 8:

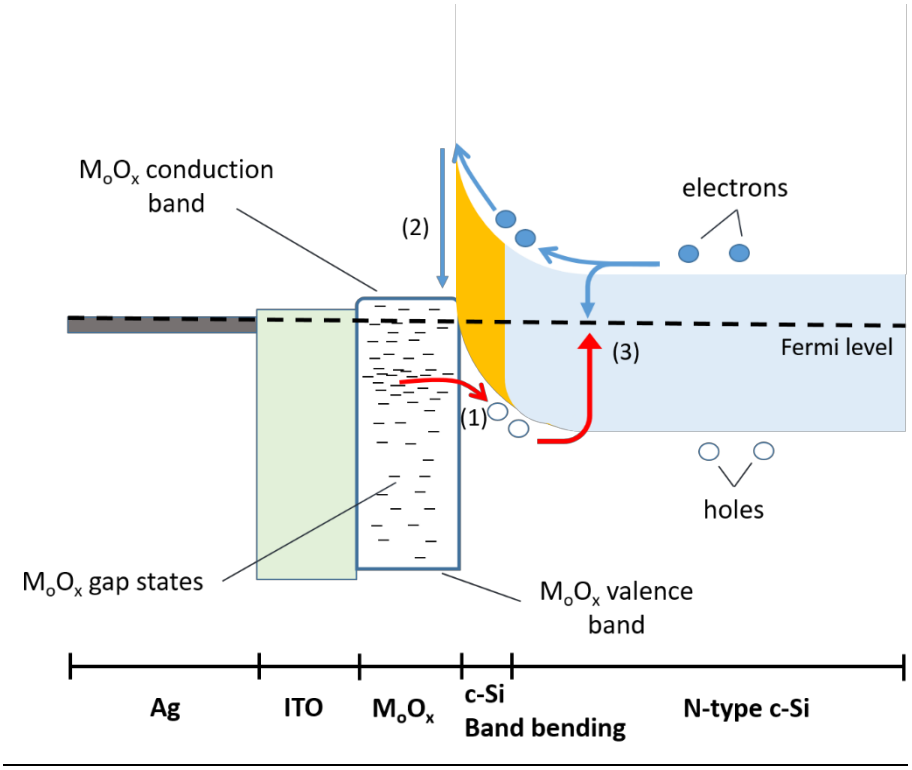
M_oO_x conduction band
(2)
electrons
(3)
Fermi level
(1)
holes
M_oO_x gap states
M_oO_x valence band
Ag
ITO
M_oO_x
c-Si
Band bending
N-type c-Si

Figure Captions:

Fig. 1. MoO_x solar cell structure fabricated for this study. The MoO_x layer acts as a hole selective contact on n-type silicon.

Fig. 2. J-V and EQE characteristic of a MoO_x based solar cell under illumination at 1 sun at room temperature.

Fig. 3. Dark J-V characteristics of the solar cell, measured (stars) and fitted (blue lines), at different temperatures, from 360 K to 220 K. The black arrow goes from the highest temperature in this study (360 K) to the lowest (220 K). The temperature difference between consecutive curves is 20 K.

Fig. 4. Exponential factor for the two conduction mechanisms predominant in the solar cell. We can observe a temperature dependence in $A_1(T)$ for the high voltage process while the low voltage process $A_2(T)$ remains almost constant.

Fig. 5. Saturation current as a function of 1000/ T for both mechanisms. We obtained an activation energy of $E_a = 0.90 \pm 0.06$ eV and $E_a = 0.30 \pm 0.01$ eV for each process.

Fig. 6. Reverse bias characteristic under dark conditions, for temperatures from 360 K to 220 K in 20K steps. The respective fits (lines) were calculated using eq. (4).

Fig.7. Ordinate intercept of the fittings of eq. (4) as a function of 1/ T for the temperature range used in this study. We obtained an activation energy of $E_a = 0.27 \pm 0.01$ eV.

Fig. 8. Proposed equilibrium band diagram of a MoO_x silicon based solar cell and the current transport mechanisms identified with numbers: (1) tunnelling mechanism, (2) Schottky barrier, (3) diffusion/recombination mechanism. The observed tunnel in reverse bias is the same than (1), but in the opposite direction.

References:

[1] K. Yoshikawa *et al.*, "Silicon heterojunction solar cell with interdigitated back contacts for a photoconversion efficiency over 26%," *Nature Energy,* Article vol. 2, p. 17032, 03/20/online 2017.

[2] W. Shockley and H. J. Queisser, "DETAILED BALANCE LIMIT OF EFFICIENCY OF P-N JUNCTION SOLAR CELLS," *Journal of Applied Physics,* vol. 32, no. 3, pp. 510-&, 1961 1961.

[3] M. A. Green *et al.*, "Solar cell efficiency tables (version 49)," *Progress in Photovoltaics,* vol. 25, no. 1, pp. 3-13, Jan 2017.

[4] Z. C. Holman *et al.*, "Current Losses at the Front of Silicon Heterojunction Solar Cells," *Ieee Journal of Photovoltaics,* vol. 2, no. 1, pp. 7-15, Jan 2012.

[5] A. Richter, S. W. Glunz, F. Werner, J. Schmidt, and A. Cuevas, "Improved quantitative description of Auger recombination in crystalline silicon," *Physical Review B,* vol. 86, no. 16, Oct 9 2012, Art. no. 165202.

[6] A. Cuevas, P. A. Basore, G. GiroultMatlakowski, and C. Dubois, "Surface recombination velocity of highly doped n-type silicon," *Journal of Applied Physics,* vol. 80, no. 6, pp. 3370-3375, Sep 15 1996.

[7] J. Bullock *et al.*, "Efficient silicon solar cells with dopant-free asymmetric heterocontacts," *Nature Energy,* vol. 1, Jan 25 2016, Art. no. 15031.

[8] J.-H. Yang *et al.*, "Dopant-Free Hydrogenated Amorphous Silicon Thin-Film Solar Cells Using Molybdenum Oxide and Lithium Fluoride," *Journal of Physical Chemistry C,* vol. 117, no. 45, pp. 23459-23468, Nov 14 2013.

[9] C. Battaglia *et al.*, "Hole Selective MoOx Contact for Silicon Solar Cells," *Nano Letters,* vol. 14, no. 2, pp. 967-971, Feb 2014.

[10] U. Wuerfel, A. Cuevas, and P. Wuerfel, "Charge Carrier Separation in Solar Cells," *Ieee Journal of Photovoltaics,* vol. 5, no. 1, pp. 461-469, Jan 2015.

[11] J. Tong, Y. Wan, J. Cui, S. Lim, N. Song, and A. Lennon, "Solution-processed molybdenum oxide for hole-selective contacts on crystalline silicon solar cells," *Applied Surface Science,* vol. 423, pp. 139-146, Nov 30 2017.

[12] D. Zielke, A. Pazidis, F. Werner, and J. Schmidt, "Organic-silicon heterojunction solar cells on n-type silicon wafers: The BackPEDOT concept," *Solar Energy Materials and Solar Cells,* vol. 131, pp. 110-116, Dec 2014.

[13] D. Zielke, C. Niehaves, W. Loevenich, A. Elschner, M. Hoerteis, and J. Schmidt, "Organic-silicon solar cells exceeding 20% efficiency," *5th International Conference on Silicon Photovoltaics, Siliconpv 2015,* vol. 77, pp. 331-339, 2015 2015.

[14] Y. Wan *et al.*, "Magnesium Fluoride Electron-Selective Contacts for Crystalline Silicon Solar Cells," *Acs Applied Materials & Interfaces,* vol. 8, no. 23, pp. 14671-14677, Jun 15 2016.

[15] M. Bivour, J. Temmler, H. Steinkemper, and M. Hermle, "Molybdenum and tungsten oxide: High work function wide band gap contact materials for hole selective contacts of silicon solar cells," *Solar Energy Materials and Solar Cells,* vol. 142, pp. 34-41, Nov 2015.

[16] J. Meyer, S. Hamwi, M. Kroeger, W. Kowalsky, T. Riedl, and A. Kahn, "Transition Metal Oxides for Organic Electronics: Energetics, Device Physics and Applications," *Advanced Materials,* vol. 24, no. 40, pp. 5408-5427, Oct 23 2012.

[17] M. Jorgensen, K. Norrman, and F. C. Krebs, "Stability/degradation of polymer solar cells," *Solar Energy Materials and Solar Cells,* vol. 92, no. 7, pp. 686-714, Jul 2008.

[18] H.-D. Um, N. Kim, K. Lee, I. Hwang, J. H. Seo, and K. Seo, "Dopant-Free All-Back-Contact Si Nanohole Solar Cells Using MoOx and LiF Films," *Nano Letters,* vol. 16, no. 2, pp. 981-987, Feb 2016.

[19] K. A. Nagamatsu *et al.*, "Titanium dioxide/silicon hole-blocking selective contact to enable double-heterojunction crystalline silicon-based solar cell," *Applied Physics Letters,* vol. 106, no. 12, Mar 23 2015, Art. no. 123906.

[20] L. G. Gerling, S. Mahato, C. Voz, R. Alcubilla, and J. Puigdollers, "Characterization of Transition Metal Oxide/Silicon Heterojunctions for Solar Cell Applications," *Applied Sciences-Basel,* vol. 5, no. 4, pp. 695-705, Dec 2015.

[21] J. Bullock, A. Cuevas, T. Allen, and C. Battaglia, "Molybdenum oxide MoOx: A versatile hole contact for silicon solar cells," *Applied Physics Letters,* vol. 105, no. 23, Dec 8 2014, Art. no. 232109.

[22] C. Battaglia *et al.*, "Silicon heterojunction solar cell with passivated hole selective MoOx contact," *Applied Physics Letters,* vol. 104, no. 11, Mar 17 2014, Art. no. 113902.

[23] J. Geissbuehler *et al.*, "22.5% efficient silicon heterojunction solar cell with molybdenum oxide hole collector," *Applied Physics Letters,* vol. 107, no. 8, Aug 24 2015, Art. no. 081601.

[24] S. R. Hammond *et al.*, "Low-temperature, solution-processed molybdenum oxide hole-collection layer for organic photovoltaics," *Journal of Materials Chemistry,* vol. 22, no. 7, pp. 3249-3254, 2012 2012.

[25] J. Meyer and A. Kahn, "Electronic structure of molybdenum-oxide films and associated charge injection mechanisms in organic devices," *Journal of Photonics for Energy,* vol. 1, 2011 2011, Art. no. 011109.

[26] K. H. Wong, K. Ananthanarayanan, J. Luther, and P. Balaya, "Origin of Hole Selectivity and the Role of Defects in Low-Temperature Solution-Processed Molybdenum Oxide Interfacial Layer for Organic Solar Cells," *Journal of Physical Chemistry C,* vol. 116, no. 31, pp. 16346-16351, Aug 9 2012.

[27] Z. Q. Liu *et al.*, "Metal-Insulator Transition in SrTiO3-x Thin Films Induced by Frozen-Out Carriers," *Physical Review Letters,* vol. 107, no. 14, Sep 28 2011, Art. no. 146802.

[28] Z. Q. Liu *et al.*, "Reversible metal-insulator transition in LaAlO3 thin films mediated by intragap defects: An alternative mechanism for resistive switching," *Physical Review B,* vol. 84, no. 16, Oct 7 2011, Art. no. 165106.

[29] M. Colina, A. B. Morales-Vilches, C. Voz, I. Martin, P. R. Ortega, and R. Alcubilla, "Low Surface Recombination in Silicon-Heterojunction Solar Cells With Rear Laser-Fired Contacts From Aluminum Foils," *Ieee Journal of Photovoltaics,* vol. 5, no. 3, pp. 805-811, May 2015.

[30] L. G. Gerling, C. Voz, R. Alcubilla, and J. Puigdollers, "Origin of passivation in hole-selective transition metal oxides for crystalline silicon heterojunction solar cells," *Journal of Materials Research,* vol. 32, no. 2, pp. 260-268, Jan 2017.

[31] T. F. Schulze, L. Korte, E. Conrad, M. Schmidt, and B. Rech, "Electrical transport mechanisms in a-Si:H/c-Si heterojunction solar cells," *Journal of Applied Physics,* vol. 107, no. 2, Jan 15 2010, Art. no. 023711.

[32] L. F. Marsal, J. Pallares, X. Correig, J. Calderer, and R. Alcubilla, "Electrical characterization of n-amorphous/p-crystalline silicon heterojunctions," *Journal of Applied Physics,* vol. 79, no. 11, pp. 8493-8497, Jun 1 1996.

[33] W. Shockley, "THE THEORY OF P-N JUNCTIONS IN SEMICONDUCTORS AND P-N JUNCTION TRANSISTORS," *Bell System Technical Journal,* vol. 28, no. 3, pp. 435-489, 1949 1949.

[34] C. T. Sah, R. N. Noyce, and W. Shockley, "CARRIER GENERATION AND RECOMBINATION IN P-N JUNCTIONS AND P-N JUNCTION CHARACTERISTICS," *Proceedings of the Institute of Radio Engineers,* vol. 45, no. 9, pp. 1228-1243, 1957 1957.

[35] H. Matsuura, T. Okuno, H. Okushi, and K. Tanaka, "ELECTRICAL-PROPERTIES OF N-AMORPHOUS P-CRYSTALLINE SILICON HETEROJUNCTIONS," *Journal of Applied Physics,* vol. 55, no. 4, pp. 1012-1019, 1984 1984.

[36] A. Vasic, M. Stojanovic, P. Osmokrovic, and N. Stojanovic, "The influence of ideality factor on fill factor and efficiency of solar cells," *Trends in Advanced Materials and Processes,* vol. 352, pp. 241-245, 2000 2000.

[37] S. Altindal, S. Karadeniz, N. Tugluoglu, and A. Tataroglu, "The role of interface states and series resistance on the I-V and C-V characteristics in Al/SnO2/p-Si Schottky diodes," *Solid-State Electronics,* vol. 47, no. 10, pp. 1847-1854, Oct 2003.

[38] R. T. Tung, "ELECTRON-TRANSPORT AT METAL-SEMICONDUCTOR INTERFACES - GENERAL-THEORY," *Physical Review B,* vol. 45, no. 23, pp. 13509-13523, Jun 15 1992.

[39] C. R. Crowell, "PHYSICAL SIGNIFICANCE OF TO ANOMALIES IN SCHOTTKY BARRIERS," *Solid-State Electronics,* vol. 20, no. 3, pp. 171-175, 1977 1977.

[40] E. H. Rhoderick and R. H. Williams, C. press, Ed. *Metal-semiconductors contacts*. 1988.

[41] L. G. Gerling *et al.*, "Transition metal oxides as hole-selective contacts in silicon heterojunctions solar cells," *Solar Energy Materials and Solar Cells,* vol. 145, pp. 109-115, Feb 2016.

[42] T. Sun *et al.*, "Investigation of MoOx/n-Si strong inversion layer interfaces via dopant-free heterocontact," *Physica Status Solidi-Rapid Research Letters,* vol. 11, no. 7, Jul 2017, Art. no. 1700107.

[43] A. R. Riben and D. L. Feucht, "NGE-PGAAS HETEROJUNCTIONS," *Solid-State Electronics,* vol. 9, no. 11-1, pp. 1055-&, 1966 1966.

[44] L. F. Marsal, I. Martin, J. Pallares, A. Orpella, and R. Alcubilla, "Annealing effects on the conduction mechanisms of p(+)-amorphous-Si0.8C0.2 : H/n-crystalline-Si diodes," *Journal of Applied Physics,* vol. 94, no. 4, pp. 2622-2626, Aug 15 2003.

[45] H. C. Card and E. H. Rhoderick, "STUDIES OF TUNNEL MOS DIODES .1. INTERFACE EFFECTS IN SILICON SCHOTTKY DIODES," *Journal of Physics D-Applied Physics,* vol. 4, no. 10, pp. 1589-+, 1971 1971.